



Investigation of localized surface plasmon resonance of nanoparticles with various shape

Tomsk Polytechnic University

Andrey Averkiev ^a

^a Research School of Chemistry & Applied Biomedical Sciences

Abstract

More and more scientific manuscripts are being published on the topic of various plasmon nanoparticles investigation by various methods, such as Raman spectroscopy, SERS, TERS, iPERS, etc. All this indicates an increased interest in the object of study and in the wide possibilities of its application in chemistry, medicine, and production.

This paper presents an analysis of the methods for studying NP and their interpretation. The proposal of our own method for investigation of NPs. 3D simulation model of a plasmonic gold nanoparticle of cubic shape. The influence of various parameters: size, direction of a plane-parallel wave and polarization angle on a change in the shape and intensity of the electric field around a plasmon nanoparticle. This article presents new approaches to the study of NP. Results of this investigation can be used for photochemistry applications and for medical use in the diagnosis and treatment of cancerous tumors.

Keywords: nanoparticles, LSPR, electromagnetic field, SERS, simulation model, therapy, diagnostics;

1. Introduction

Nowadays, one of the most extensively exploited features of metallic NPs is the localized surface plasmon resonance (LSPR), which refers to the collective oscillation of electrons on the metallic NPs excited by the incident photons at the resonant frequency. The excitation of LSPR bands enables the enhanced and tunable electromagnetic fields, light absorption and scattering based on the physical and elemental parameters of NPs, which in turn holds the promise of enhanced device performances. When the sizes of the metal nanoparticle (MeNPs) are smaller than the wavelength of irradiating electromagnetic (EM) radiation used for excitation the electromagnetic field of the incident light exert a force on the free conduction electrons inside MeNPs and displace them to the one side to the surface of MeNPs creating a relatively positive charge on another side. As a result, the electric dipoles are created, which have net electric field opposite to the incident electric field and provide restoring force to the displaced electron. In that way these electrons started oscillation inside the MeNPs and act as a quantum oscillator. The electrons inside NPs always oscillating with a specific natural frequency called plasmonic frequency. When the frequency of incident EM radiation matches the plasma frequency, it generates localized surface plasmon resonance (LSPR) mode. A secondary photon may be released from the excited electron in the NPs, which is called

scattered photon. The MeNPs have very high absorption and scattering cross section in the region where LSPR occurs [10].

Nowadays, there are several reports that highlight possible methods of various LSPR applications.

2. Materials and methods

Authors analyze the hot carrier distribution and dynamics that result from SMA and LSPR excitation by computing the instantaneous populations of orbitals both above and below the Fermi level of the metal nanostructure [9].

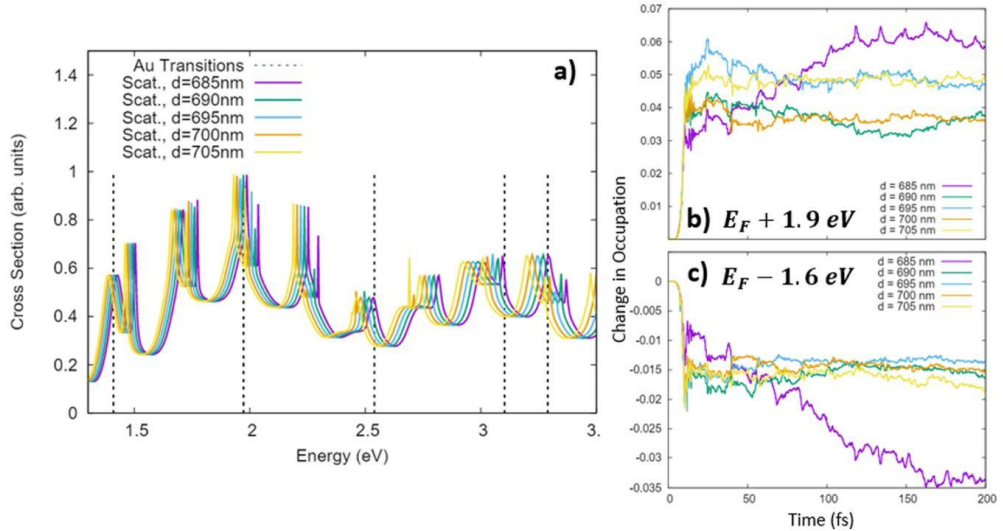


Figure 1. Fine-shaping of the spatial and temporal profile of the incident field through the geometry of the dielectric nanosphere. Panel (a) shows the scattering spectra of a size progression of dielectric nanospheres. The 685 nm nanosphere’s scattering spectrum has the best overlap with the dipole-allowed transitions in the $L = 2$ nm PIW Au NC model. This structure shows the most efficient generation of hot electrons in the most energetic orbitals included in our active space (panel b) and more efficient generation of hot holes in the lowest energy orbitals included in the PIW Au NC active space (panel c) [9].

Jason et al. [9] choose Au and Pt because the SMA phenomenon has been experimentally demonstrated in both metals. Some authors (Sun, [6]) considered SiO_2 nanospheres decorated with Pt nanoparticles of size similar to the particles considered in this report [9]. Zhang et al., [5] considered TiO_2 nanospheres decorated with large Au nanoparticles. It has been shown that band structure effects have less of an impact on hot carrier dynamics in Ag nanoparticles due to the relatively large (>3 eV) gap between the d-bands and the Fermi level [2, 11]. Analogous calculations have been performed on Ag-decorated nanospheres showing qualitative features similar to the results with Au and Pt (Figure 1). The ability to drive excited-state dynamics of hot carriers through tuning of these resonances may have important implications for improving the efficiency and selectivity of photocatalysis via hot carrier transfer, which can be severely limited by the rapid decay of energetic carriers resulting from plasmon resonances [9].

Surface-enhanced Raman spectroscopy (SERS) is a unique optical phenomenon that can improve the Raman signal of molecules millions of times and has gained more attention within the last forty years [7, 8]. Electromagnetic (EM) enhancement is one of two widely accepted SERS enhancement mechanisms which amplifies the Raman signal of the probed molecules adjacent to the local electric field due to the surface plasmon resonance (SPR) effect [7, 13].

The recent development of plasmonic metal with a semiconductor nanocomposite has given a new direction to the photovoltaic and photocatalytic applications, where charge carriers can be generated on semiconductor surface through decay of localized surface plasmon [4].

Authors [3] demonstrate the absorption of visible-light, near-IR photons and SHE with an electronically integrated $\text{AgTiO}_2\text{-AuNR}$ composite. Silver is responsible for harvesting high energy photons in the violet-blue region. AuNR is responsible for harvesting the low-energy photons in green to near-IR region. At present, the major hurdle in the AuNR-TiO₂ system, for the SWS application, is the surfactant removal from the AuNR surface without applying any high temperature calcination. The surfactant molecules at the interface of the AuNRs and TiO₂ is known to hinder the charge transfer (CT) property between metal NPs and semiconductor [12]. The CT is affected because of the low conductivity of organic component and the significant distance between AuNP and semiconductor due to the interleaving surfactant molecules. This decreases the intensity of LSPR induced electromagnetic field near the semiconductor, and hence the full advantage of plasmon effect was not utilized for applications. These fields are nonhomogeneous in nature. The intensity is the maximum at the surface of the metal NPs and decreases exponentially with distance from the surface [3].

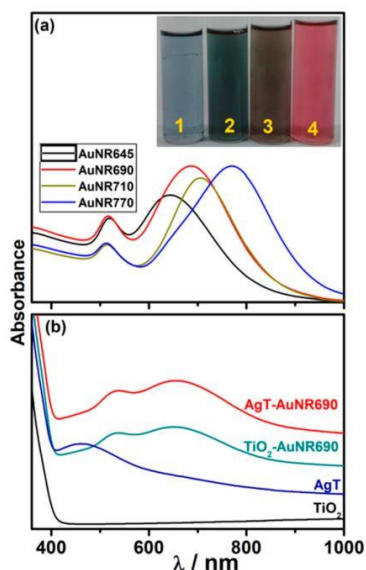


Figure 2. (a) UV-visible absorption spectra of different aspect ratios of AuNRs and inset displays a change in color with increase in aspect ratio of Au NR. 1, 2, 3, and 4 in the inset correspond to the longitudinal absorption maximum of AuNRs at 645, 690, 710, and 770 nm, respectively. (b)

UV-visible absorption spectra of TiO₂, AgT, TiO₂-AuNR690, and AgT-AuNR690 .

AuNR with four different aspect ratios (length to diameter ratio) was synthesized by seed-mediated method. UV-visible absorption spectrum recorded for Au NRs is shown in Figure 2a. The asymmetrical nature of Au NR splits the plasmon resonance frequency into two modes, with one along the transverse axis and the other along the longitudinal axis. The polarization along the transverse axis shows a narrow and low-intensity plasmon resonance peak at 520 nm, and the polarization along the longitudinal axis shows a high-intensity and broad plasmon resonance peak at higher λ , which strongly depends on the aspect ratio of NR. As shown in Figure 2a, the longitudinal plasmon resonance shifted to the higher wavelength with increasing silver content. The UV-visible spectra of AgT show a broad plasmon absorption band between 400 and 480 nm. Four TiO₂, four AgT and AuNRs were prepared by loading a different aspect ratio of NR. The

longitudinal and transverse plasmon resonance of AuNR is also visible after incorporation of TiO₂ and AgT. Representative results for TiO₂-AuNR690 and AgT-AuNR690 are shown in Figure 3b [3].

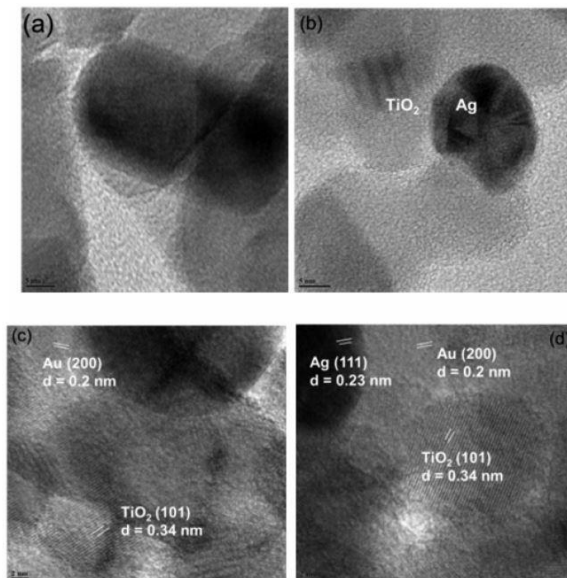


Figure 3. HRTEM images of (a) TiO₂-AuNR and (b) AgT composites are shown. The heterojunction between AgNPs and TiO₂ is demonstrated from the TEM image. (c,d) AuNR deposited on AgT is evident from the d value shown in HRTEM images. Note the junctions observed between all three components of Ag, TiO₂, and AuNR in panel d. Scale bar is 5 nm (a,b) and 2 nm (c,d) [3].

Chinnakonda et al. [3] states that significant decrease is clearly seen in the transverse absorption area, while under longitudinal absorption it increased from AuNR690 to 770. HRTEM analysis shows the (200) planes on the longitudinal axis of AuNRs. The morphology and microstructural property of the AgT-AuNR-x (x = 645, 690, 710, 770, corresponding to longitudinal absorption maximum of AuNR) nanocomposites was explored by HRTEM, and the results are shown in Figure 3.

Four different catalysts were prepared by loading AuNR with different aspect ratio on AgTiO₂, and surfactant was removed by HClO₄ treatment. In contrast, only 448 and 630 $\mu\text{mol/h}\cdot\text{g}$ of H₂ was produced from TiO₂-AuNR690 and AgT, respectively, under one sun illumination, as shown in Figure 4a. In the case of TiO₂-AuNR, the high-energy photons (400–500 nm) were utilized to a lower extent due to low absorption coefficient (refer to Figure 4). This results in a decrease in the activity compared with AgT-AuNR. The reason is that AuNR is not in direct contact with TiO₂ as well as no heterojunction is present as evident from the Raman spectroscopy and TEM results. The activity of H₂ evolution under one sun condition is attributed to the near-field effect of AuNR [3].

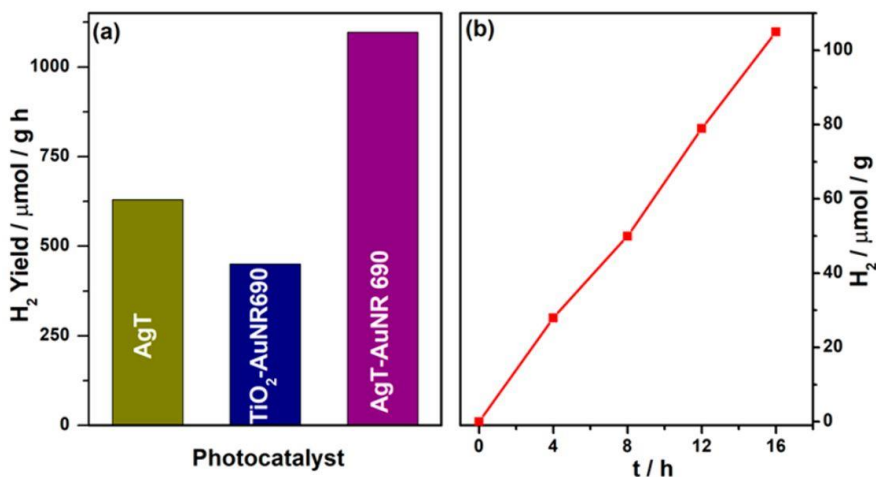


Figure 4. (a) Photocatalytic H₂ evolution over AgT, TiO₂-AuNR690, and AgT-AuNR690 catalyst in aqueous methanol solution under one sun illumination and (b) hydrogen yield as a function of time for AgT-AuNR690 under $\lambda \geq 550$ nm light irradiation [3].

To verify the longitudinal plasmon contribution, the reaction was carried out with low-energy photons ($\lambda \geq 550$ nm). The maximum H₂ production of 7 $\mu\text{mol}/\text{h}\cdot\text{g}$ was achieved with AgT-AuNR690 and AgT-AuNR710 catalyst. Under these conditions, we can safely assume that no visible-light contribution to SWS arises from the LSPR effect of AuNR along the transverse axis. This suggests that only the longitudinal plasmon of AuNR is involved in the photocatalytic H₂ evolution. The H₂ evolution reaction was carried out with 550 nm cut off filter for 16 h, and a linear increase in H₂ amount was observed, as shown in Figure 4b [3].

It should be noted that although the energy harvested exclusively from near-IR region is very small, it demonstrates a significantly large amount of solar light harvesting when combined with other high-energy green and blue photons under one sun conditions. Longitudinal absorption of AuNR690 occurs effectively between 580 and 800 nm. Indeed, it absorbs both high-energy visible and low-energy NIR photons with high absorption coefficient. This leads to more hot electrons as well as NIR harvesting simultaneously. Hence the high activity was observed, whereas the extent of such synergistic light absorption is less with other size nanorods.

3. Discussion

In this section, we will consider the 3D model simulation results. In a previous article, a model of a spherical nanoparticle was already disclosed and described [1]. This article presents investigation of a cubic nanoparticle. This model was obtained in the commercial environment of COMSOL Multiphysics, electromagnetic module, frequency domain. The model was investigated on the effect of changes in the size of nanoparticles (10 and 100 nm) and various polarization vectors on the shape and intensity of the scattered electric field caused by LSPR. All studies were conducted with a constant wavelength of 650 nm. Mesh remained a constant triangular shape for PML, a tetrahedral shape for other model objects. Mesh had a predefined in program size: “normal” for PML, “extra small” for air, and “extremely small” for cubic nanoparticle. The material for the cubic nanoparticle was selected from the COMSOL Multiphysics integrated library and was gold «Johnson and Christie 1972».

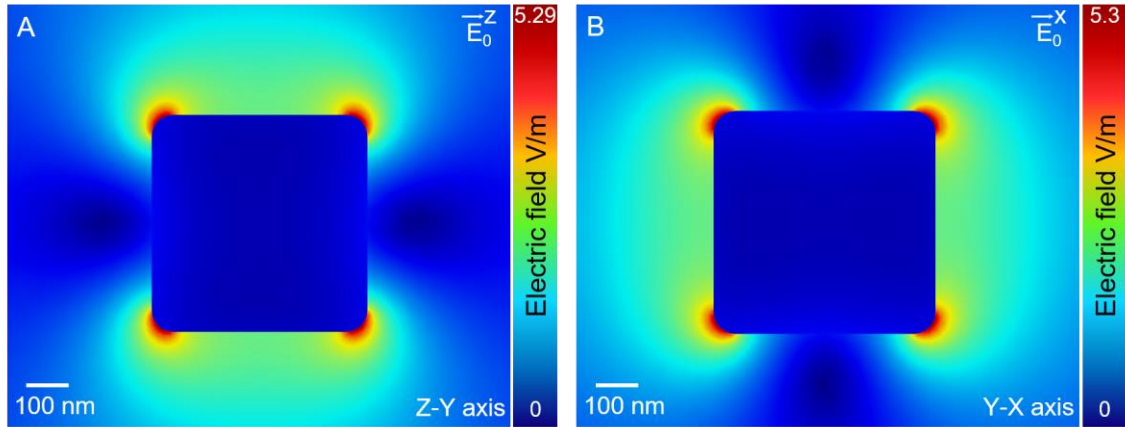


Figure 5. 3D simulation model of electric field enhancement around nanocube with a side of 100 nm. Material of cube is Au (Johnson and Christy 1972): A) Plane parallel wave with wavelength of 650 nm (red light) goes along X axis, polarization is along vertical Z axis with the maximum of $5.29 \cdot 10^4$ [V/m]; B) Plane parallel wave with wavelength of 650 nm drops from top to bottom and polarization is in horizontal X-axis with the maximum of $5.3 \cdot 10^4$ [V/m].

Figure 5 shows the LSPR scattering of the electric field by a cubic nanoparticle with dimensions of 100x100 nm and rounded faces with a radius of 10 nm. It can be observed that in both cases (A and B), the distributed field is a dipole located vertically in the case of Figure 5 A and horizontally in the case of Figure 5 B. You can see the concentration of the maximum field intensity on the rounded faces of the nanocube as expected. Numerically the maximum field values practically coincide (5.29 V/m for A and 5.3 V/m for B). The difference between the maximum values is 0.01 V/m, which is included in the engineering error. We can say that changing only the direction of laser radiation or a plane-parallel wave, as in our case, will change the direction of polarization, but will not change the shape and intensity of the electric field.

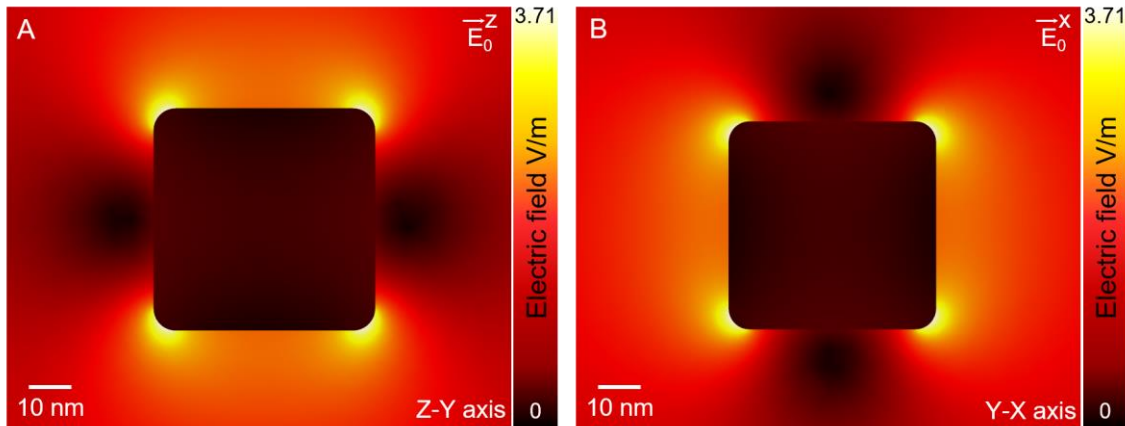


Figure 6. 3D simulation of scattered electric field around nanocube with side of 10 nm. Nanocube material is Au (Johnson and Christy 1972). Wavelength of plane parallel wave was 650 nm: A) Wave goes along X axis with vertical Z polarization. Maximum of scattered electric field was $3.71 \cdot 10^4$ [V/m]; B) Wave drops from top to bottom along Z axis with horizontal X polarization. Maximum of scattered electric field was $3.71 \cdot 10^4$ [V/m].

Figure 6 shows the LSPR scattering of the electric field by a cubic nanoparticle with a size of 10x10 nm and rounded faces with a radius of 1 nm. As we see in both cases (A and B), the

distributed field is a dipole located vertically in the case of Figure 6 A and horizontally in the case of Figure 6 B. As in the case of Figure 5, we can see the concentration of the maximum field strength on the rounded nanocube edges. Numerically the maximum field values coincide for A and B and are equal to 3.71 V/m. However, it should be noted that the maximum values of the electric field in Figures 6A, B are less than the values obtained in Figures 5A, B. This suggests that in contrast from the direction of laser irradiation or a wave that does not affect the shape and size of the field a change in the size of the nanoparticle and, in particular, its decrease from 100 to 10 nm helps to reduce the electric field by about 1.5 times from the same shape.

4. Conclusion

In this manuscript, several scientific works were studied showing on the LSPR effect using various techniques of Raman spectroscopy and the possibility of using LSPR. Our own study of the LSPR phenomenon was presented in the form of a simulation model of a cubic nanoparticle. The obtained model demonstrates the scattering of a plane-parallel wave in the form of the electric field intensity increase around the nanoparticle, which is a direct consequence of the LSPR effect.

The data obtained allow us to draw the following conclusions: a change in the direction of a plane-parallel wave changes only the direction of the polarization vector of the nanoparticle while a change in the size of the nanoparticle reduces the intensity of the electric field with its shape unchanged.

This change in field intensity may be critical for the use of cubic nanoparticles in the diagnosis of cancerous tumors. With a reduced intensity of the electric field, it will be more difficult (or not at all possible) to establish the place of plasmon nanoparticles accumulation, and hence the accumulation of cancer cells. Also, the scattered field may not be enough to heat the surrounding area to a sufficient temperature to destroy cancer cells (41-43 °C) during photothermal therapy. In this regard, in medical applications, namely theranostics of cancerous tumors, it is advisable to use nanoparticles of 100 nm or more size.

References:

1. Averkiev, A.A. (2019). Analysis of plasmonic nanoparticles applications and their influence on scattered electric field. *Journal of Economics and Social Sciences*. №. 15. pp. 6-13.
2. Atwater, H. A., Narang, P., Sundararaman, R.(2016). Plasmonic hot carrier dynamics in solid-state and chemical systems for energy conversion. *Nanophotonics*. 5. pp. 96–11.
3. Chinnakonda, S. Gopinath and Kshirodra Kumar Patra†. (2018). Harnessing Visible-Light and Limited Near-IR Photons through Plasmon Effect of Gold Nanorod with AgTiO₂. *J. Phys. Chem.* 122. pp. 1206–1214.
4. Christopher, P., Ingram, D.B., Linic, S. (2011). Plasmonic-Metal Nanostructures for Efficient Conversion of Solar to Chemical Energy. *Nat. Mater.* 10. pp. 911–921.
5. Claverie, J.P., Jin, X., Liu, H., Morales-Guzman, P.I., Razzari, L., Yu, X., Zhang, H., Zhang, J.(2016). Engineering the Absorption and Field Enhancement Properties of Au-TiO₂ Nanohybrids via Whispering Gallery Mode Resonances for Photocatalytic Water Splitting. *ACS Nano* 2016. 10. pp. 4496–4503.
6. Codrington, J., Foley, J. J., Gray, S. K., Han, C., Sun, Y., Xu, Y.-J., Zhang, D., Zhang, N. (2016). Near-field dielectric scattering promotes optical absorption by platinum nanoparticles. *Nat. Photonics* 2016. 10. pp. 473–482.
7. Etchegoin, P. & Le, R. E. Principles of surface-enhanced Raman spectroscopy. (2008). [Available at <https://www.elsevier.com/books/principles-of-surface-enhanced-raman-spectroscopy/le-ru/978-0-444-52779-0>] [Viewed on 20.03/2020]

8. Fleischmann, M., Hendra, P. J. & McQuillan, A. J. (1974). Raman spectra of pyridine adsorbed at a silver electrode. *Chem. Phys. Lett.* 26. Issue 2. pp. 163–166.
9. Jason Codrington, Jonathan J. Foley, Kimberly Fernando and Noor Eldabagh. (2017). Unique Hot Carrier Distributions from Scattering-Mediated Absorption. *ACS Photonics* 2017. 4. pp. 552–559.
10. Krull, U. J. & Petryayeva, E. (2011). Localized surface plasmon resonance: Nanostructures, bioassays and biosensing - A review. *Analytica Chimica Acta.* 706(1). pp. 8–24.
11. Kulkarni, V., Liu, J. G., Manjavacs, A., Nordlander, P. (2014). Plasmon-Induced Hot Carriers in Metallic Nanoparticles. *ACS Nano* 2014. 8. pp. 7630–7638.
12. Liu, L., Ouyang, S., Ye, J. (2013). Gold-nanorod-Photosensitized Titanium dioxide with Wide-Range Visible-Light Harvesting Based on Localized Surface Plasmon Resonance. *Angew. Chem., Int. Ed.* 2013. 52. pp. 6689–6693.
13. Schlücker, S. (2014). Surface-enhanced Raman spectroscopy: concepts and chemical applications. *Angew. Chem. Int. Ed.* 53. pp. 4756–4795.